



**HAL**  
open science

## **YbPO 4 nano-cylinders formation and alignment within optical fiber preforms using fiber-drawing process**

C. Kinowski, H. El Hamzaoui, B. Capoen, G. Bouwmans, Anne-Marie Blanchenet, K. Delplace, B. Prochet, M. Bouazaoui

### ► **To cite this version:**

C. Kinowski, H. El Hamzaoui, B. Capoen, G. Bouwmans, Anne-Marie Blanchenet, et al.. YbPO 4 nano-cylinders formation and alignment within optical fiber preforms using fiber-drawing process. Materials Research Bulletin, 2018, 97, pp.293 - 299. 10.1016/j.materresbull.2017.09.014 . hal-01596236

**HAL Id: hal-01596236**

**<https://hal.science/hal-01596236>**

Submitted on 15 Jul 2024

**HAL** is a multi-disciplinary open access archive for the deposit and dissemination of scientific research documents, whether they are published or not. The documents may come from teaching and research institutions in France or abroad, or from public or private research centers.

L'archive ouverte pluridisciplinaire **HAL**, est destinée au dépôt et à la diffusion de documents scientifiques de niveau recherche, publiés ou non, émanant des établissements d'enseignement et de recherche français ou étrangers, des laboratoires publics ou privés.

## Accepted Manuscript

Title: YbPO<sub>4</sub> nano-cylinders formation and alignment within optical fiber preforms using fiber-drawing process

Authors: C. Kinowski, H. El Hamzaoui, B. Capoen, G. Bouwmans, A.-M. Blanchenet, K. Delplace, B. Prochet, M. Bouazaoui



PII: S0025-5408(17)32132-3  
DOI: <http://dx.doi.org/10.1016/j.materresbull.2017.09.014>  
Reference: MRB 9554

To appear in: *MRB*

Received date: 30-5-2017  
Revised date: 3-9-2017  
Accepted date: 8-9-2017

Please cite this article as: C.Kinowski, H.El Hamzaoui, B.Capoen, G.Bouwmans, A.-M.Blanchenet, K.Delplace, B.Prochet, M.Bouazaoui, YbPO<sub>4</sub> nano-cylinders formation and alignment within optical fiber preforms using fiber-drawing process, Materials Research Bulletin <http://dx.doi.org/10.1016/j.materresbull.2017.09.014>

This is a PDF file of an unedited manuscript that has been accepted for publication. As a service to our customers we are providing this early version of the manuscript. The manuscript will undergo copyediting, typesetting, and review of the resulting proof before it is published in its final form. Please note that during the production process errors may be discovered which could affect the content, and all legal disclaimers that apply to the journal pertain.

## YbPO<sub>4</sub> nano-cylinders formation and alignment within optical fiber preforms using fiber-drawing process

C. Kinowski<sup>\*1</sup>, H. El Hamzaoui<sup>1</sup>, B. Capoen<sup>1</sup>, G. Bouwmans<sup>1</sup>, A.-M. Blanchenet<sup>2</sup>, K. Delplace<sup>1</sup>, B. Prochet<sup>1</sup> and M. Bouzaoui<sup>1</sup>.

<sup>1</sup> Univ-Lille, CNRS, UMR 8523 - PhLAM - Physique des Lasers Atomes et Molécules, CERLA/IRCICA, F-59000 Lille, France

<sup>2</sup> Univ-Lille, CNRS, UMR 8207 – UMET – Unité Matériaux et Transformations, F-59000 Lille, France

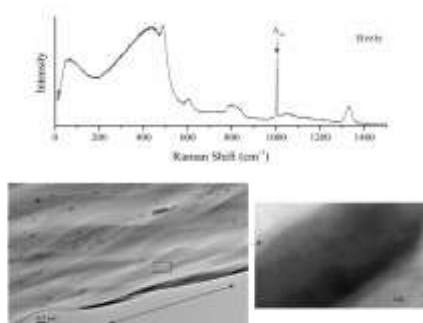
\* Corresponding author: Christophe Kinowski

Tel: (33)320434818

Fax: (33)320337020

Email address: [christophe.kinowski@univ-lille1.fr](mailto:christophe.kinowski@univ-lille1.fr)

Graphical abstract



### Highlights

- Synthesis of YbPO<sub>4</sub> nano- nanoparticles and nano-cylinders within optical fiber preforms using a sol-gel process.
- Structural analyses confirm that tetragonal YbPO<sub>4</sub> nanocrystals had grown in the matrix.
- The nanoparticles evolve to form nano-cylinders after drawing.
- These nano-cylinders are all aligned parallel to the rod-drawing direction.
- These glass ceramics exhibit a structured absorption spectra around 980 nm, which corroborates the Yb<sup>3+</sup> crystalline environment.

**Abstract**

This paper describes the first synthesis of YbPO<sub>4</sub> nano-cylinders and nanoparticles within optical fiber preforms. To obtain YbPO<sub>4</sub>-doped silica monoliths, phosphosilicate powders, previously prepared by a sol-gel method, were impregnated with a solution containing an ytterbium salt. Then, they were compressed into cylinders and sintered at high temperature. These doped monoliths were densified under controlled atmosphere and then drawn at high temperature into 1.6 mm diameter-rods. The composition, structural and optical properties of these monoliths and rods were investigated using Electron Probe Micro-Analysis, Transmission Electron Microscopy (TEM), Raman spectroscopy and IR absorption measurements. The size of the YbPO<sub>4</sub> nanoparticles within the monoliths were found to be in the range of 8-15 nm and 13-25 nm, depending on the Yb-doping amount. Upon drawing the most concentrated Yb-doped monoliths into rods, the nanoparticles evolve to form nano-cylinders with a mean diameter around 40 nm and a length of about 400 nm. Similar behavior was observed for the less concentrated Yb-doped monoliths, once drawn into rods but a lower number of nano-cylinders were found in this case. Structural analysis, based on Raman spectroscopy and TEM experiments, shows that all these nano-objects have a tetragonal xenotime structure (*I4<sub>1</sub>/amd*). Moreover, it was found that the nano-cylinders were all aligned parallel to the drawing direction. These SiO<sub>2</sub>-P<sub>2</sub>O<sub>5</sub>:YbPO<sub>4</sub> glass ceramics exhibit a structured absorption spectra around 980 nm, which corroborates the Yb<sup>3+</sup> crystalline environment.

**Keywords:** A. nanostructures, A. optical materials, B. sol-gel chemistry, C. Raman spectroscopy, C. transmission electron microscopy (TEM)

**1. Introduction**

In recent years, glass-ceramics containing lanthanide orthophosphates (LnPO<sub>4</sub>; Ln =lanthanide) nano-objects have attracted considerable attention, far beyond the materials

science and condensed-matter communities, due to their potential applications in different fields. These materials present interesting properties such as excellent ultraviolet (UV) transparency, high refractive index ( $\sim 1.8$ ), high thermal stability, very low solubility in water and high solubility of rare-earth elements [1,2]. These properties are the root of increasing interest in lanthanide orthophosphates for a wide range of applications such as phosphors [1,3-4], proton-conducting solid oxide fuel cells (SOFCs) [5], catalysts [6] or for their intriguing magnetic properties and phase transitions at low temperatures [7-8].

In the past few years, several kinds of  $\text{LnPO}_4$  nano-objects, such as core-shell nano-composites [9], microspheres [3] or hollow microspheres [4], nanorods [10] have been obtained using various solution synthesis routes, among which hydrothermal synthesis [4,9], chemical precipitation method [10], sol-gel method [1,6], spray pyrolysis procedure [3] can be mainly cited. The obtained nano-objects were thereafter used in solution or collected and heat-treated at different temperatures to use them in the various applications mentioned above.

Recently, an important research effort has been deployed throughout the world to develop methods for the preparation and the design of optical fiber preforms or optical fibers doped with oxide nanostructures [11-20]. The main aim of this research is to achieve the next generation of efficient optical fiber amplifiers and lasers as well as their hardening against ionizing radiations for space applications [16, 17]. One of these methods, developed by Draka company (France) [11-14] and Naval research Laboratory (Washington DC, USA) [15], is based on the synthesis of  $\text{Al}_2\text{O}_3:\text{Er}^{3+}$  or  $\text{AlPO}_4:\text{Yb}^{3+}/\text{Er}^{3+}$  nanoparticles (NP) by co-precipitation approach. These nanoparticles were incorporated into the silica preforms prepared by MCVD (Modified Chemical Vapour Deposition), which were then drawn into fibers. Under the condition of identical opto-geometrical parameters, it was shown that the NP-based fibers always outperform their standard counterparts in terms of amplification factor [11-14], laser efficiency [15,18] or resistance to ionizing radiation [16,17]. The second

approach, proposed by LPMC (Nice, France) [19-20], is also based on MCVD synthesis, except that the authors use the thermal treatments inherent to MCVD process to generate NP through the phase separation mechanism. In this way, the NP are generated in-situ within the material during the sintering treatment after alkaline-earth ions (Mg, Ca and Sr) have been incorporated into the fiber preform core. Hence, the two approaches rely on the conventional MCVD process and on the solution doping technique.

In this paper, we report, for the first time to our best knowledge, the synthesis of  $\text{YbPO}_4$  nanoparticles and nano-cylinders within optical fiber preforms using a sol-gel process. The structural and optical properties of the obtained samples have been studied using Raman spectroscopy, high-resolution transmission electron microscopy (HRTEM) and absorption spectroscopy.

## 2. Experimental

Porous phosphosilicate powder was obtained from xerogels prepared using the already reported sol-gel process [21]. Sets of this powder were then post-doped by impregnation using ytterbium nitrate in ethanol solution at different concentrations. Then, the powders were dried at  $120^\circ\text{C}$ . The doped powdered samples were mechanically compressed to get cylindrical rods. After that, they were submitted to dehydration under chlorine/oxygen atmosphere and densification at  $1200^\circ\text{C}$  for two hours under helium atmosphere, as described elsewhere [22]. The obtained glass rods have diameters of about 12 mm. Eventually, the obtained doped glass rods were drawn into 1.6 mm-diameter canes at about  $2000^\circ\text{C}$ . The feed rate and draw speed were 8mm/min and 0.28m/min respectively. No further heat-treatment was performed on these canes.

Electron Probe Micro-Analysis (EPMA) was performed on cut and polished slices of preforms or canes using a CAMECA SX 100 microprobe.

Transmission electron microscopy (TEM) images were recorded with a FEI Tecnai G220 microscope operating at 200 kV. To this purpose, several microscope grids were prepared following two different procedures, depending on the need to observe NP orientation. If such observation is not needed or for a preliminary experiment, pieces of the samples were simply grinded into fine powder and deposited onto a 200 mesh copper grid covered by a carbon membrane. In the case of the determination of nano-cylinders orientation, a cut slice of the rod was first mechanically polished down to a thickness of *ca.* 30  $\mu\text{m}$ . The sample was then glued on a hollow grid and then put in a low-angle ion milling system (PIPS, Gatan) to reach electron transparency. In both cases, the grid was finally metallized using a sputtered carbon film.

The polarized micro-Raman spectra were obtained in a confocal configuration using a triple-grating spectrometer (Jobin Yvon T64000) and the 514.5 nm line of an  $\text{Ar}^+$  laser as the excitation source with a power level of 50 mW (measured at the sample). All Raman spectra were recorded at room temperature in the wavenumber range 10–1500  $\text{cm}^{-1}$  with a spectral resolution of 1  $\text{cm}^{-1}$ . A 10 $\times$  objective was used for all micro-Raman experiments, focusing the laser to a spot of 2.5  $\mu\text{m}$  in diameter.

Prior to the optical measurements, 1 mm-thick pieces from the monoliths were cut and polished to obtain optical quality. NIR absorption spectra were obtained at room temperature using a Cary 5000 double-beam spectrophotometer (Agilent Technologies) in the range 800–1100 nm with a spectral resolution of 0.02 nm.

### 3. Results and discussion

Before proceeding further, EPMA was performed in order to control ytterbium and phosphorus concentration profiles into monoliths and rods (not shown). In both cases, the phosphorus and ytterbium radial concentrations were found homogenous. The phosphorus concentration was  $2.00 \pm 0.10$  wt% whereas the ytterbium concentration depended on the initial concentration of the doping solution. We have studied samples with two different Yb contents: one having a concentration of  $0.30 \pm 0.05$  wt% (called SiP0.3) and the other characterized by a concentration of  $1.50 \pm 0.15$  wt% (called SiP1.5).

### 3.1 Optical absorption

Absorption spectra of the SiP0.3 and SiP1.5 monoliths are shown in Fig. 1, corresponding to the  ${}^2F_{7/2} \rightarrow {}^2F_{5/2}$  of  $\text{Yb}^{3+}$  ions.

These spectra, which are similar in shape each other, are very different from those usually obtained in pure silica glass or phosphate glass [23-26], even in phosphosilicate optical fiber [27]. Many components are clearly observed in these absorbance spectra, which can be explained through the Stark splitting of the sub-levels due to the crystal-field in a crystalline environment of ytterbium ions [28-30]. The maximum  $\text{Yb}^{3+}$ -related absorptions at 975 nm (zero-phonon line) present an attenuation level of 124 and 680  $\text{dB.m}^{-1}$  for the SiP0.3 and SiP1.5 monoliths, respectively. At this wavelength, the absorption cross section, deduced from this measurements and using the ytterbium concentration obtained from EPMA, is estimated to be  $(1.30 \pm 0.15) \times 10^{-20} \text{ cm}^2$ . This value is close to the one reported for Yb-doped phosphosilicate glasses  $(1.4 \pm 0.1) \times 10^{-20} \text{ cm}^2$  [31].

### 3.2 Raman spectroscopy

In order to be able to identify the crystalline phase, polarized micro-Raman investigations were performed. Raman spectrum obtained in the VV configuration (Vertical-Vertical polarization, also called polarized configuration) of the SiP1.5 monolith is presented in Fig. 2.

This spectrum is characteristic of vitreous phosphosilicate glasses. In the low-wavenumber region, the band appearing around  $60\text{ cm}^{-1}$  and called the Boson peak is one of the universal characteristics of glasses. According to the “non-continuous random structure” model of Duval *et al* [32], this band can be interpreted as reflecting the acoustic vibration of cohesive domains. The band around  $430\text{ cm}^{-1}$  is attributed to the bending modes  $\delta(\text{Si-O-Si})$  of the polymerized structure of amorphous silicate. The sharp bands  $D_1$  and  $D_2$  peaking at  $\sim 490$  and  $\sim 604\text{ cm}^{-1}$ , known as defect modes, have been associated to symmetric breathing vibrations of oxygen atoms in four- and three-membered silica rings, respectively [33]. The asymmetric band situated around  $800\text{ cm}^{-1}$  is assigned to a complex vibration involving substantial silicon motion in addition to a bending movement of oxygen in a vitreous network [34-36]. The high-frequency region is dominated by an intense band at  $1327\text{ cm}^{-1}$  which is attributed to the symmetric stretching vibration of P=O bonds whereas shoulders localized at  $720\text{ cm}^{-1}$  and  $1130\text{ cm}^{-1}$  are assigned to the O=P-O bending mode and P-O-P stretching mode, respectively. These last three bands are characteristic of vibrations involving phosphorus motion in a phosphosilicate glass network [37, 38]. As they cannot be observed in crystalline phase, these bands attest the presence of phosphorous atoms in the amorphous matrix. However, several peaks (indexed by asterisks) appear in the Raman spectrum: they are localized at  $1003\text{ cm}^{-1}$ ,  $1023\text{ cm}^{-1}$  and  $1064\text{ cm}^{-1}$ , which could not be attributed to the vitreous matrix. Since the  $\delta(\text{Si-O-Si})$  band is strongly polarized, its contribution can be eliminated from spectra recorded in the HV configuration (Horizontal-Vertical polarization, also called depolarized configuration) in order to intensify the crystalline peaks. Fig. 3 exhibits the Raman spectrum of the same

sample SiP1.5 in the HV configuration. In addition, Raman spectra of undoped phosphosilicate and Suprasil F300 (Heraeus) are presented for comparison.

In this depolarized configuration, we could observe a set of eight peaks only for the SiP1.5 monolith. These peaks are assigned to Raman modes of YbPO<sub>4</sub> crystals. Indeed, ytterbium orthophosphate, in the same way as several other lanthanide phosphates RPO<sub>4</sub> (R = Tb, Dy, Ho, Er, Tm and Lu) and as xenotime (YPO<sub>4</sub>), crystallizes in the tetragonal zircon structure. The crystal belongs to space group  $D_{4h}^{19}$  ( $I4_1/amd$ ). The primitive cell contains two YbPO<sub>4</sub> formula units, i.e. 12 atoms. Group theory predicts twelve Raman active modes for the zircon structure of YbPO<sub>4</sub> with A<sub>1g</sub>, B<sub>1g</sub>, B<sub>2g</sub> and (doubly degenerated) E<sub>g</sub> symmetries, corresponding to the following Raman (polarizability) tensor components [39]:

$$A_{1g} = \begin{pmatrix} xx & & \\ & yy & \\ & & zz \end{pmatrix} \quad B_{1g} = \begin{pmatrix} xx & & \\ & -yy & \\ & & \end{pmatrix}$$

$$B_{2g} = \begin{pmatrix} & xy & \\ yx & & \\ & & \end{pmatrix} \quad E_g = \begin{pmatrix} & & xz \\ & & yz \\ zx & zy & \end{pmatrix}$$

Seven of these modes ( $2A_{1g} + 2B_{1g} + 1B_{2g} + 2E_g$ ) are usually labeled as internal modes due to normal vibrations of oxygen atoms in the (PO<sub>4</sub>)<sup>3-</sup> units, four modes ( $2B_{1g} + 2E_g$ ) are referred to external modes arising from translations of (PO<sub>4</sub>)<sup>3-</sup> and Yb<sup>3+</sup> ions. Finally, one mode (E<sub>g</sub>) is the rotation mode of the whole (PO<sub>4</sub>)<sup>3-</sup> units [39]. According to polarized Raman measurements on single-oriented YbPO<sub>4</sub> crystals [40, 41], the wavenumber values of the observed Raman modes  $\bar{\nu}$ , their symmetry and character assignments are given in Table 1.

It should be noticed that not all expected Raman-active modes are observed in our experimental spectra. Vibration bands associated with the translation modes, normally present below  $300\text{ cm}^{-1}$ , do not appear in both VV and HV polarized Raman spectra. Indeed, the low-frequency Boson peak of the glass matrix, which is not sensitive to polarization effect, probably hides the translational vibrations of ytterbium orthophosphate crystals. Moreover, according to the tensor component of the  $A_{1g}$  species, this Raman mode is totally symmetric and consequently very sensitive to polarization effect. From the intensities of the Raman band at  $1003\text{ cm}^{-1}$  recorded in both polarizations, the depolarization ratio  $I_{HV}/I_{VV}$  has been calculated and is equal to 0.07, closed to zero as expected. It must be mentioned first that Raman spectra recorded in HV and VV polarizations did not depend on the orientation of the sample under the incident laser beam. On the other hand, similar spectra were acquired in the case of the SiP0.3 monolith, except that those spectra exhibit crystal peaks with lower intensities.

Raman spectroscopic investigations were also conducted on the millimeter-sized rods drawn at  $2000^\circ\text{C}$ , doped with 0.3 wt% and 1.5 wt% ytterbium ions. The observed spectra were initially found similar to those associated with monoliths. However, the presence of the crystal vibration bands and/or their intensities was highly dependent on the sample orientation. These results led us to hypothesize the presence of oriented crystals within the rods along their drawing direction. In order to confirm our hypothesis, polarized Raman spectra were recorded by controlling the orientation of the millimeter-sized rod and the laser beam polarization. Since  $\text{YbPO}_4$  crystallizes in the tetragonal phase, we will first assume that

the  $c$  axis of the crystallites will be defined along the drawing axis so that  $a$  and  $b$  axes will define the basal plane. Thereafter, the scattering configuration will be indicated by adopting the Porto's notation [42], namely  $\mathbf{k}_i(\mathbf{e}_i\mathbf{e}_s)\mathbf{k}_s$  where  $\mathbf{k}_i$  and  $\mathbf{k}_s$  are the propagation directions of incident and scattered beams, respectively, while  $\mathbf{e}_i$  and  $\mathbf{e}_s$  designate the corresponding electric field unit vectors. Hence, the next notations  $x$ ,  $y$  and  $z$  will coincide with the crystallographic axes  $a$ ,  $b$  and  $c$ . Since the micro-polarized Raman measurements were performed in backscattering geometry ( $180^\circ$ ), it allowed us to record spectra in the following three polarizations:  $\bar{y}(xx)y$ ,  $\bar{y}(zz)y$  and  $\bar{y}(xz)y$  (with  $\bar{y} = -y$ ), where the crystal modes ( $A_{1g} + B_{1g}$ ),  $A_{1g}$  and  $E_g$  are respectively expected.

Fig. 4 exhibits the micro-polarized  $\bar{y}(xx)y$  and  $\bar{y}(zz)y$  Raman spectra of the SiP1.5 millimeter-sized rod.

Both spectra are similar to the one in Fig. 2, mainly characteristic of vitreous phosphosilicate glasses, since the selected polarizations in Fig. 4 are equivalent to the VV configuration used for the monolith analyzes. However, in the  $\bar{y}(zz)y$  Raman spectrum, only a strong and sharp peak at  $1003\text{ cm}^{-1}$  can be observed, corresponding to the  $A_{1g}$  symmetry mode of the  $\text{YbPO}_4$  crystal, as expected from the tensor components. This is in accordance with our assumption that the polarization directions of the incident and scattered light are parallel to millimeter-sized rod axis, i.e. to the  $c$  axis of the crystals. It should be noticed that the second  $A_{1g}$  mode, which should appear at  $486\text{ cm}^{-1}$ , could not be observed due to the overlapping with the vibration band associated with the  $D_1$  vibration mode of the silica glass network. On the contrary, in the  $\bar{y}(xx)y$  configuration, both incident and scattered polarizations are perpendicular to the drawing axis of the millimeter-sized rod, i.e. perpendicular to the  $c$  crystal axis. As expected, both  $A_{1g}$  and  $B_{1g}$  symmetry modes are observed in the

corresponding Raman spectrum. In the  $\bar{y}(xz)y$  configuration, only the  $E_g$  symmetry mode is expected to appear, according to the tensor components.

Actually, in Fig. 5 showing the Raman spectrum in this configuration, the three sharp peaks at  $298\text{ cm}^{-1}$ ,  $578\text{ cm}^{-1}$  and  $1022\text{ cm}^{-1}$  are assigned to this  $E_g$  symmetry mode. However, three less intense additional peaks appear in the spectrum, corresponding to the  $A_{1g}$  and  $B_{1g}$  modes. This partial mixing of the tensor components can originate from the depolarization of the laser radiation inside the crystal, which could give rise to a substantial spillover of forbidden modes. These symmetry modes thus appear together with the expected ones. This effect has been already observed, even in the case of pure lanthanide orthophosphate monocrystals [43-45]. Once again, it should be mentioned that similar results have been found in the case of a 0.3 wt%  $\text{Yb}^{3+}$ -doped rod (SiP0.3).

In summary, from this micro-polarized Raman spectroscopy study, it can be argued that ytterbium orthophosphate crystallites are presents within the phosphor-silicate matrices. While in the case of bulk monoliths, crystals are formed in random directions, their  $c$ -axis is mainly oriented along the rod-drawing direction in millimeter-sized rods.

### 3.3 Structure and morphology of the crystals

In order to confirm the presence of crystallites within monoliths and rods as well as to identify the morphology of these particles, TEM analysis was performed. As shown in Fig. 6a and Fig. 6b, SiP0.3 and SiP1.5 monoliths exhibit several particles with sizes in the ranges 8-15 nm and 13-25 nm, respectively. In the case of the SiP0.3 sample, it should be noticed that the particles density is weaker, due to the lower concentration of ytterbium. Fig. 6c displays a typical TEM micrograph of a nanocrystal in high-resolution (HRTEM) within the SiP1.5 monolith.

These nanoparticles show inter-reticular spacing of  $(3.48 \pm 0.10)$  Å, which is in good agreement with the distance between the (200) planes of the tetragonal phase of  $\text{YbPO}_4$  (JCPDS 00-45-0530). Energy dispersion X-ray (EDX) analysis was carried out in scanning mode (STEM mode) with a 6 nm-diameter probe beam. Fig. 7 shows the corresponding EDX spectra taken inside (Fig. 7a) the nanocrystal of Fig. 6c and far (Fig. 7b) from this particle.

The peaks assigned to copper are ascribable to the microscope grid, the detected carbon element obviously comes from the grid membrane and from the sputtered conductive film. Silicon and oxygen are coming from the matrix. The EDX spectrum of the particle (Fig. 7a) contains peaks assigned to phosphorus and ytterbium whereas no trace of this latter element (Yb) was detected far from the particle (Fig. 7b). These results confirm the presence of  $\text{YbPO}_4$  nanocrystals into monoliths and the chemical composition of the phosphosilicate glass matrix. It should be stressed that EDX spectra have been taken in STEM mode with a 6 nm-diameter probe beam and also with a probe volume which is difficult to control. Furthermore, as the sample thickness depends on the probe location, a quantitative analysis would have been hazardous. However, the presence of the phosphorous peak, even outside of any nanocrystal, shows that some phosphorous atoms remain in the matrix.

Fig. 8 exhibits typical TEM and HRTEM micrographs of nanocrystals within the SiP1.5 millimeter-sized rod. Unlike what is found in monoliths, nano-cylinder-shaped particles can be observed with lengths in the range 40-400 nm and mean diameters in the range 20-60 nm. It should be noticed that monocrytalline nanocrystals were mainly observed in several HRTEM micrographs.

These cylinders are mainly oriented in the rod-drawing direction, symbolized by a double arrow. The HRTEM image shows inter-reticular spacing of  $(4.54 \pm 0.08) \text{ \AA}$ , which is in good agreement with the distance between the (101) planes of  $\text{YbPO}_4$  in tetragonal phase. EDX analyses performed on a nano-cylinder and far from any particles (Fig. 9) confirm the chemical compositions of both the  $\text{YbPO}_4$  nano-cylinders and the phosphosilicate glass matrix. In the same way, analyses carried out on the SiP0.3 millimeter-sized rod yielded the same results, except a lower nano-cylinders density observed within this sample.

Vermillac *et al* have recently reported elongation and break-up of particles during the drawing process [46]. The authors have shown that, during the drawing process of a Ge-doped fiber containing  $\text{LaF}_3:\text{Tm}^{3+}$  nanoparticles, the flow of the materials and viscous stresses may induce deformation of the particles into long threads. Moreover, particles having initial diameters between 140 and 200 nm inside the preform can break-up in fragments with diameters down to 60 nm inside the drawn fiber, which was presented as a strategy to obtain small particles within an optical fiber. In our study, we cannot explain the formation of nano-cylinders exactly by the same mechanism since nano-cylinders are larger than the initial particles within the preforms. Since the drawing temperature ( $2000^\circ\text{C}$ ) is higher than the melting temperature of such rare-earth orthophosphate crystals [47], the melting of some  $\text{YbPO}_4$  nanoparticles within the preforms is likely. Hence, the most probable mechanism after this melting is that liquid bubbles of  $\text{YbPO}_4$  coalesce to give large particles and since the drawing speed (0.28 m/min) is slower than that used for drawing optical fiber (around 50m/min), the liquid matter is transformed into crystalline phase. The nano-rod shape of the resulting particles can be

easily explained by viscous stress and flow alignment during the liquid stage, like in the case of  $\text{LaF}_3$  particles [46].

## Conclusion

Absorbance, EPMA, TEM and polarized micro-Raman measurements have been carried out on phosphosilicate systems containing 2 wt% phosphorus and two different ytterbium concentrations (0.3 and 1.5 wt%). Investigations have been performed on monoliths and on their corresponding drawn-rods. Absorbance measurements have shown the presence of  $\text{Yb}^{3+}$  ions in crystalline environment. Structural analyses, based on polarized micro-Raman spectroscopy and TEM, have confirmed that tetragonal  $\text{YbPO}_4$  nanocrystals had grown in the matrix. These nanocrystals have no particular shape within the densified monoliths before drawing step, with sizes in the range 8-15 nm and 13-25 nm for the lower and higher Yb-doping content, respectively. After the drawing of these monoliths into rods, the nanoparticles evolve to form nano-cylinders with length in the range 40-400 nm and a mean diameter in the range 20-60 nm. Moreover, these nano-cylinders are all aligned parallel to the rod-drawing direction. A better understanding of the nano-cylinders formation is necessary to tailor the size of these nano-objects within the rod. This step, which will lead us to achieve optical fibers with controlled  $\text{YbPO}_4$  nano-rods inside the core, will be the subject of a further study. However, the present results are very promising for the development of nano-glass-ceramic optical fibers with aligned nano-cylinders. Incorporation of rare-earth ions inside nanocrystals in the fiber core is known to improve the resistance of the fiber to photodarkening under high power laser excitation. Furthermore, for a given volume of doping crystal, elongation and orientation along the fiber axis are desirable in order to reduce light scattering.

## Acknowledgements

We would like to thank S. Plus for technical assistance. This work has been supported by IRCICA ([www.ircica.univ-lille1.fr](http://www.ircica.univ-lille1.fr)) and CERLA institutes of University of Lille. This work has been partially founded by the Agence Nationale de la Recherche through the NANOFIBER project (ANR-12-RMNP-0019), the LABEX CEMPI (ANR-11-LABX-0007) and the Equipex Flux (ANR-11-EQPX-0017), as well as by the Ministry of Higher Education and Research, Hauts de France Regional Council and European Regional Development Fund (ERDF) through the Contrat de Projets Etat-Region (CPER Photonics for Society P4S). The TEM facility in Lille (France) is supported by Hauts de France Regional Council and by the European Regional Development Fund (ERDF).

## References

- [1] K. Kajihara, S. Yamaguchi, K. Kaneko, K. Kanamura, Highly transparent bright green sol-gel-derived monolithic silica-(Tb,Ce)PO<sub>4</sub> glass-ceramic phosphors, *RSC Adv.* 4 (2014) 26692-26696.
- [2] E.A. Savel'ev, K.M. Golant, Influence of fusing on the uniformity of the distribution of Yb<sup>3+</sup> ions and the formation of clusters in silica with phosphorus admixture synthesized by SPCVD, *Opt. Mat. Express* 5 (10) (2015) 2337-2346.
- [3] J. Garcia-Sevillano, E. Cantelar, A. Justo, M. Ocana, F. Cusso, LaPO<sub>4</sub>:Er microspheres with high NIR luminescent quantum yield, *Mater. Chem. Phys.* 138 (2-3) (2013) 666-671.
- [4] X. Li, H. Bi, Template-free synthesis of LaPO<sub>4</sub>:Eu<sup>3+</sup> hollow spheres with enhanced luminescent properties, *J. Alloys Compd.* 532 (2012) 72-77.
- [5] S. Phadke, J.C. Nino, M.S. Islam, Structural and defect properties of the LaPO<sub>4</sub> and LaP<sub>5</sub>O<sub>14</sub>-based proton conductors, *J. Mater. Chem.* 22 (2012) 25388-25394.
- [6] K. Ramesh, J.E. Zheng, E.G.Y. Ling, Y.F. Han, A. Borgna, Synthesis, Characterization, and Catalytic Activity of Uniformly Crystalline LaPO<sub>4</sub> Nanofiber Catalysts for Ethanol Dehydration, *J. Phys. Chem. C* 113 (37) (2009) 16530-16537.
- [7] G. K. Liu, C. K. Loong, F. Trouw, M. M. Abrahamand, L. A. Boatner, Spectroscopic studies of magnetic transitions in TbPO<sub>4</sub>, *J. Appl. Phys.* 75 (10) (1994) 7030-7032.
- [8] A. U. Miillert, J. Jakelsu, H.G. Kahle, Extensive studies on the low-temperature properties of TbPO<sub>4</sub>. III. Birefringence measurements and mean-field calculations, *J. Phys.: Condens. Matter.* 5 (7) (1993) 955-970.

- [9] X. Y. Kuang, H. Liu, W. Y. Huand, Y. Z. Shao, Hydrothermal synthesis of core–shell structured  $\text{TbPO}_4:\text{Ce}^{3+}@\text{TbPO}_4:\text{Gd}^{3+}$  nanocomposites for magnetic resonance and optical imaging, *Dalton Trans.* 43 (2014) 12321-12328.
- [10] M. Saraf, P. Kumar, G. Kedawat, J. Dwivedi, S. A. Vithayathil, N. Jaiswal, B. A. Kaiparettu, B. K. Gupta, Probing Highly-Luminescent Europium Doped Lanthanum Orthophosphate Nanorods for Strategic Applications, *Inorg. Chem.* 54 (2015) 2616–2625.
- [11] A. Pastouret, C. Gonnet, C. Collet, O. Cavani, E. Burov, C. Chanéac, A. Carton, J.P. Jolivet, Nanoparticle doping process for improved fibre amplifiers and lasers, *Proc. of SPIE* 7195 (2009) 71951X.
- [12] A. Le Sauze, C. Simonneau, A. Pastouret, D. Gicquel, L. Bigot, S. Choblet, A.M. Jurdyc, B. Jacquier, D. Bayart, L. Gasca, Nanoparticle Doping Process: Towards a Better Control of Erbium Incorporation in MCVD Fibers for Optical Amplifiers, *Proceedings of Optical Amplifiers and Their Applications Conference* (2003) WC5.
- [13] D. Boivin, A. Pastouret, E. Burov, C. Gonnet, O. Cavani, S. Lempereur, P. Sillard, C. Goldmann, E. Saudry, C. Chanéac, A. Shlifer, U. Ghera, Core-shell nanoparticle erbium-doped fibers for next generation amplifiers, *Proc. of SPIE* 8237 (2012) 82372T.
- [14] D. Boivin, A. Pastouret, E. Burov, C. Gonnet, O. Cavani, S. Lempereur, P. Sillard, Performance characterization of new erbium-doped fibers using MCVD nanoparticle doping process, *Proc. of SPIE* 7914 (2011) 791423.
- [15] C. C. Baker, E. J. Friebele, C. G. Askins, M. P. Hunt, B. A. Marcheschi, J. Fontana, J. R. Peele, W. Kim, J. Sanghera, J. Zhang, R. K. Pattnaik, L. D. Merkle, M. Dubinskii, Y. Chen, I. A. Dajani and C. Mart, Nanoparticle doping for improved Er-doped fiber lasers, *Proc. of SPIE* 9728 (2015) 97280T.

- [16] J. Thomas, M. Myara, L. Troussellier, E. Burov, A. Pastouret, D.Boivin, G. Mélin, O. Gilard, M. Sotom, P.Signoret, Radiation-resistant erbium-doped-nanoparticles optical fiber for space applications, *Opt. Express* 20 (3) (2012) 2435-2444.
- [17] R. Dardaillon, J. Thomas, M. Myara, S. Blin, A. Pastouret, C. Gonnet, P. Signoret, BroadBand Radiation-Resistant Erbium-Doped Optical Fibers for Space Applications, *IEEE Transactions on Nuclear Science* (2017) DOI: 10.1109/TNS.2017.2701550.
- [18] I. Savelii, L. Bigot, B. Capoen, C. Gonnet, C. Chanéac, E. Burova, A. Pastouret, H. El Hamzaoui, M. Bouazaoui, Benefit of Rare-Earth “Smart Doping” and Material Nanostructuring for the Next Generation of Er-Doped Fibers, *Nanoscale Res. Lett.* 12 (2017) 1-8.
- [19] W. Blanc, B. Dussardier, Formation and applications of nanoparticles in silica optical fibers, *J. Opt.* 45 (3) (2016) 247-254.
- [20] F. d'Acapito, W. Blanc, B. Dussardier, Different  $\text{Er}^{3+}$  environments in Mg-based nanoparticle-doped optical fibre preforms, *J. Non-Cryst.Solids* 401 (2014) 50–53.
- [21] H. El Hamzaoui, M. Bouazaoui, B. Capoen, Raman investigation of germanium- and phosphorus-doping effects on the structure of sol–gel silica-based optical fiber preforms, *J. Mol. Struct.* 1099 (2015) 77-82.
- [22] H. El Hamzaoui, L. Courthéoux, V. Nguyen, E. Berrier, A. Favre, L. Bigot, M. Bouazaoui, B. Capoen, From porous silica xerogels to bulk optical glasses: The control of densification, *Mater. Chem. Phys.* 121 (2010) 83-88.
- [23] A. Baz, H. El Hamzaoui, I. Fsaifes, G. Bouwmans, M. Bouazaoui, L. Bigot, A pure silica ytterbium-doped sol–gel-based fiber laser, *Laser Phys. Lett.* 10 (5) (2013) 055106.

- [24] P. Barua, E.H. Sekiya, K. Saito, A.J. Ikushima, Influences of  $\text{Yb}^{3+}$  ion concentration on the spectroscopic properties of silica glass, *J. Non-Cryst. Solids* 354 (42-44) (2008) 4760-4764.
- [25] L. Zhang, H. Hu, Evaluation of spectroscopic properties of  $\text{Yb}^{3+}$  in tetraphosphate glass, *J. Non-Cryst. Solids* 292 (1-3) (2008) 108-114.
- [26] L. Wang, H. Zeng, B. Yang, F. Ye, J. Chen, G. Chen, A. T. Smith, L. Sun, Structure-Dependent Spectroscopic Properties of  $\text{Yb}^{3+}$ -Doped Phosphosilicate Glasses Modified by  $\text{SiO}_2$ , *Materials* 10 (2) (2017) 241-249.
- [27] S. Suzuki, H. A. McKay, X. Peng, L. Fu, L. Dong, Highly ytterbium-doped silica fibers with low photo-darkening, *Opt. Express* 17 (12) (2009) 9924-9932.
- [28] P. Golewska, A. Matraszek, L. Macalik, K. Hermanowicz, M. Ptak, P.E. Tomaszewski, Spectroscopic and structural properties of  $\text{Na}_3\text{RE}(\text{PO}_4)_2:\text{Yb}$  orthophosphates synthesised by hydrothermal method (RE = Y, Gd), *J. Alloys Comp.* 628 (2015) 199-207.
- [29] A. Yoshikawa, G. Boulon, L. Laversenne, H. Canibano, K. Lebbou, A. Collombet, Y. Guyot, T. Fukuda, Growth and spectroscopic analysis of  $\text{Yb}^{3+}$ -doped  $\text{Y}_3\text{Al}_5\text{O}_{12}$  fiber single crystals, *J. Appl. Phys.* 94 (9) (2003) 5479-5488.
- [30] R. Ternane, M. Ferid, Y. Guyot, M. Trabelsi-Ayadi, G. Boulon, Spectroscopic properties of  $\text{Yb}^{3+}$  in  $\text{NaYbP}_2\text{O}_7$  diphosphate single crystals, *J. Alloys Comp.* 464 (1-2) (2008) 327-331.
- [31] M.A.Melkumov, I.A.Bufetov, M.M.Bubnov, K.S.Kravtsov, S.L.Semjonov, A.V.Shubin, E.M.Dianov, Ytterbium Lasers Based on  $\text{P}_2\text{O}_5$ - and  $\text{Al}_2\text{O}_3$ -doped Fibers, ECOC'2004 (2004) Th1.3.2.
- [32] E. Duval, A. Mermet, N.V. Surovtsev, A.J. Dianoux, Boson peak nanostructure and relaxation of glasses, *J. Non-Cryst. Solids* 235–237 (1998) 203–207.

- [33] R.A. Barrio, F.L. Galeener, E. Martinez, R.J. Elliot, Regular ring dynamics in AX<sub>2</sub> tetrahedral glasses, *Phys. Rev. B* 48 (21) (1993) 15672-15689.
- [34] R.J. Bell, The dynamics of disordered lattices, *Rep. Prog. Phys.* 35 (1972) 1315-1409.
- [35] P. Dean, The Vibrational Properties of Disordered Systems: Numerical Studies, *Rev. Mod. Phys.* 44 (1972) 127-168.
- [36] F.L. Galeener, A.E. Geissberger, Vibrational dynamics in <sup>30</sup>Si-substituted vitreous SiO<sub>2</sub>, *Phys. Rev. B* 27 (10) (1983) 6199-6204.
- [37] N. Shibata, M. Horigudhi, T. Edahiro, Raman spectra of binary high-silica glasses and fibers containing GeO<sub>2</sub>, P<sub>2</sub>O<sub>5</sub> and B<sub>2</sub>O<sub>3</sub>, *J. Non Cryst. Solids* 45 (1) (1981) 115-126.
- [38] V.G. Plotnichenko, V.O. Sokolov, V.V. Koltashev, E.M. Dianov, On the structure of phosphosilicate glasses, *J. Non Cryst. Solids* 306 (2002) 209-226.
- [39] P. Dawson, M. M. Hargreave, G. R. Wilkinson, The vibrational spectrum of zircon (ZrSiO<sub>4</sub>), *J. Phys. C: Solid State Phys.* 4 (2) (1971) 240-256.
- [40] G.M. Begun, G.W. Beall, L.A. Boatner, W.J. Gregor, Raman spectra of the rare earth orthophosphates, *J. Raman Spectrosc.* 11 (4) (1981) 273-278.
- [41] E. Nakazawa, M. Hirano, Ion–Ion and Ion–Lattice Interactions in the Optical Spectra of YbPO<sub>4</sub> Crystal, *J. Phys. Soc. Jpn.* 80 (1) (2011) 014713.
- [42] T.C. Damen, S.P.S. Porto, B. Tell, Raman Effect in Zinc Oxide, *Phys. Rev.* 142 (2) (1966) 570-574.
- [43] M. Giarola, A. Sanson, A. Rahman, G. Mariotto, Vibrational dynamics of YPO<sub>4</sub> and ScPO<sub>4</sub> single crystals: An integrated study by polarized Raman spectroscopy and first-principles calculations, *Phys. Rev. B* 83 (22) (2011) 224302.
- [44] A. Sanson, M. Giarola, M. Bettinelli, A. Speghini, G. Mariotto, Polarized micro-Raman spectroscopy and ab initio phonon modes calculations of LuPO<sub>4</sub>, *J. Raman Spectrosc.* 44 (10) (2013) 1411-1415.

- [45] A. Tatsi, E. Stavrou, Y.C. Boulmetis, A.G. Kontos, Y.S. Raptis, C. Raptis, Raman study of tetragonal  $\text{TbPO}_4$  and observation of a first-order phase transition at high pressure, *J. Phys. Condens. Mater.* 20 (42) (2008) 425216.
- [46] M. Verillac, J.F Lupi, F. Peters, M. Cabié, P. Vennéguès, C. Kucera, T. Neisius, J. Ballato, W. Blanc, Fiber-draw-induced elongation and break-up of particles inside the core of a silica-based optical fiber, *J. Am. Ceram. Soc.* 100 (5) (2017) 1814-1818.
- [47] Y. Hikichi, T. Nomura, Melting temperatures of monazite and xenotime, *J. Am. Ceram. Soc.* 70 (10) (1987) 252-253.

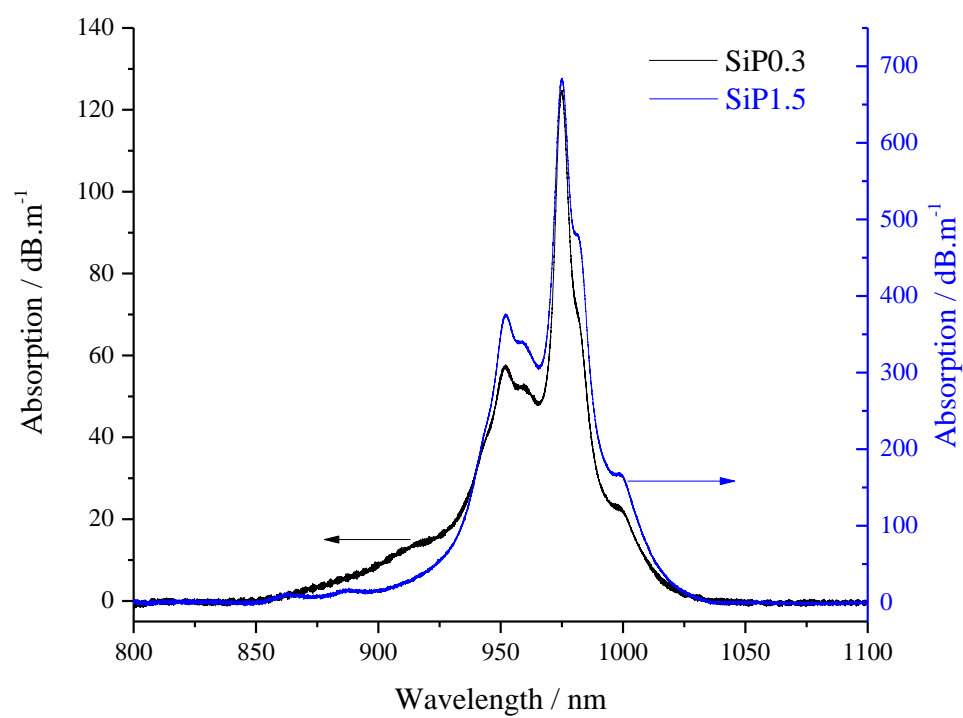


**Fig. 1.** Absorption spectra of SiP0.3 and SiP1.5 monoliths.

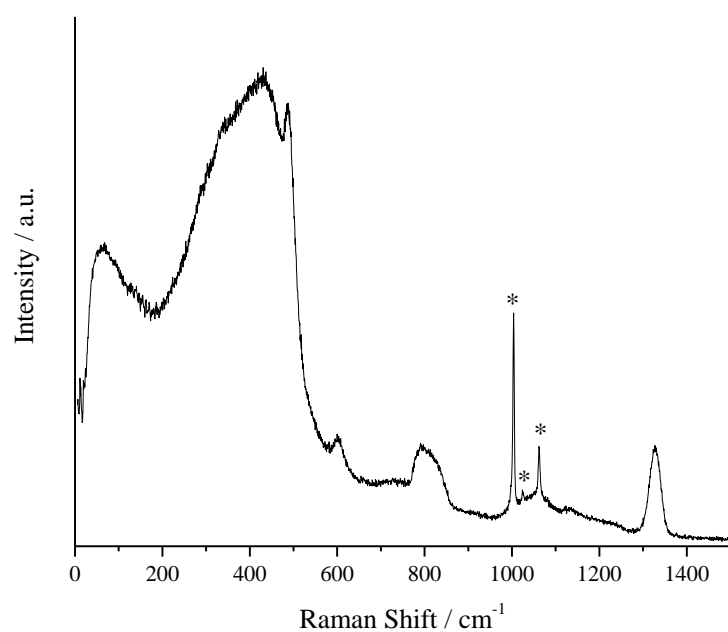


**Fig. 2.** VV micro-polarized Raman spectrum of the SiP1.5 monolith.

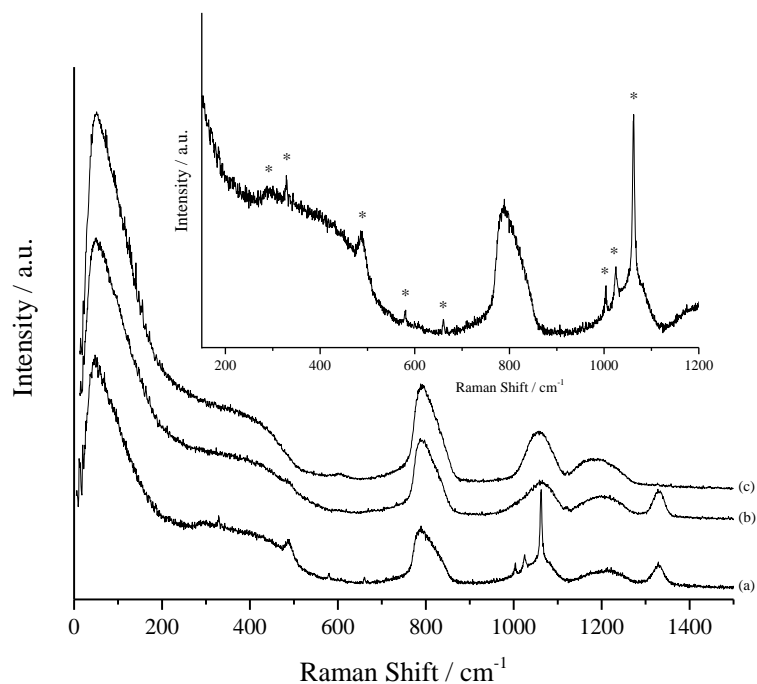


**Fig. 3.** HV micro-polarized Raman spectrum of SiP1.5 monolith (a), undoped phosphosilicate monolith (b) and Suprasil F300 (Heraeus). Inset: focus on the interesting part of the spectrum of SiP1.5 monolith.

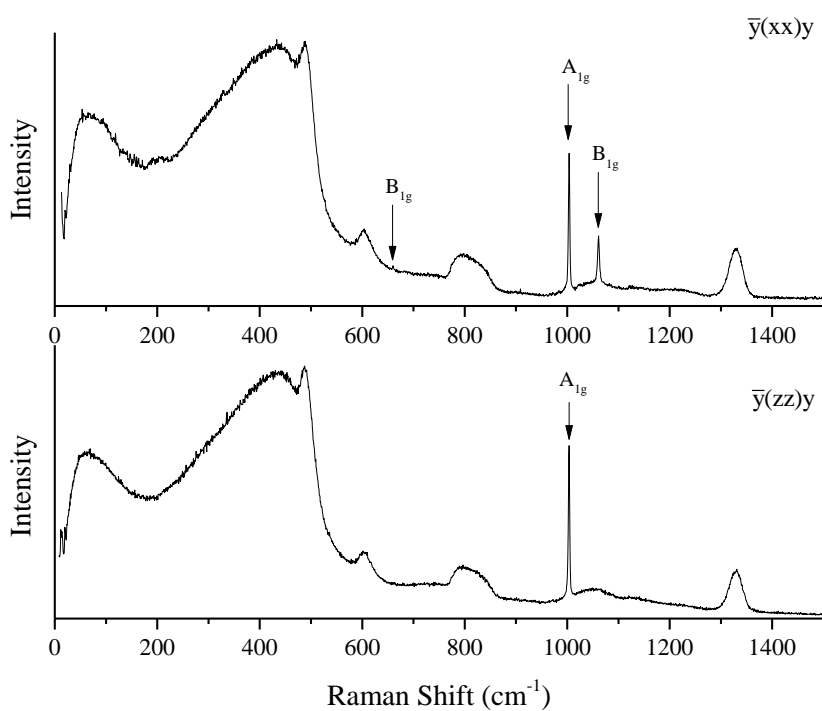


**Fig. 4.** Micro polarized  $\bar{y}(xx)y$  and  $\bar{y}(zz)y$  Raman spectra of the SiP1.5 millimeter-sized rod.

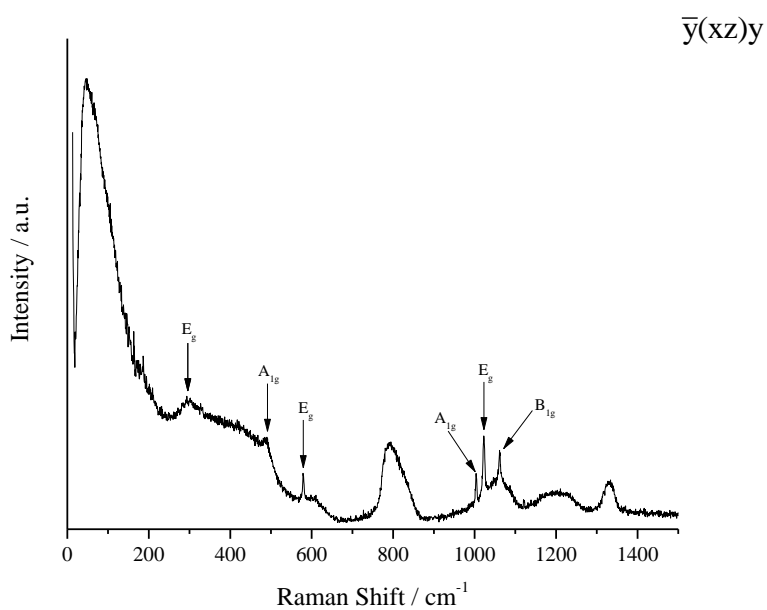


**Fig. 5.** Micro-polarized  $\bar{y}(xz)y$  Raman spectrum of the SiP1.5 millimeter-sized rod.

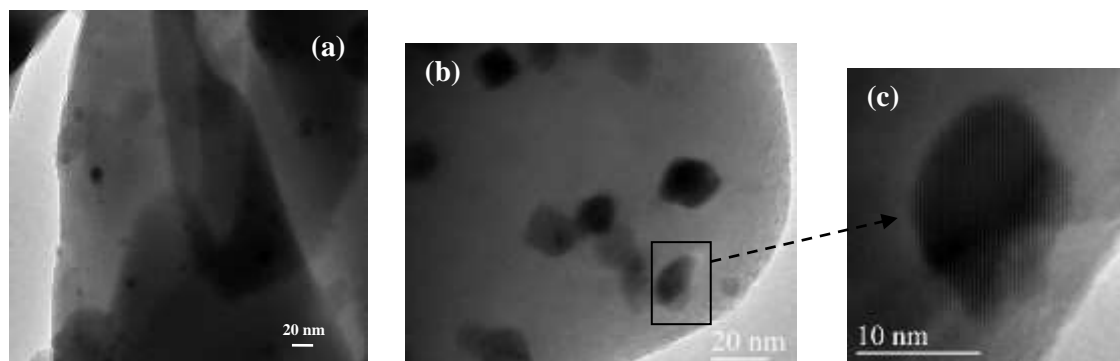


**Fig. 6.** TEM micrographs of nano-crystals within the SiP0.3 (a) and SiP1.5 (b) monoliths. Typical HRTEM micrograph of a nano-crystal (c).

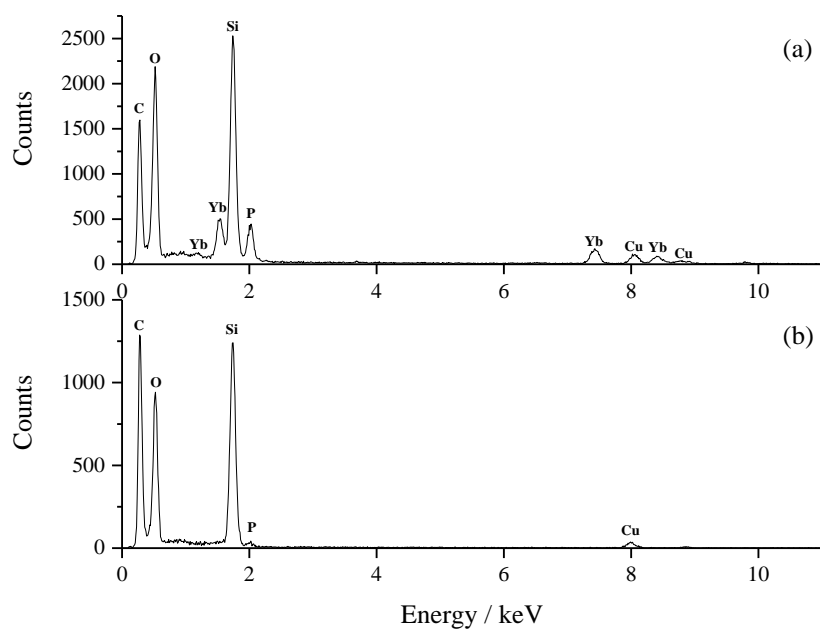


**Fig. 7.** EDX spectra taken in scanning mode (STEM): in the nanocrystal (a) and far from this particle (b).

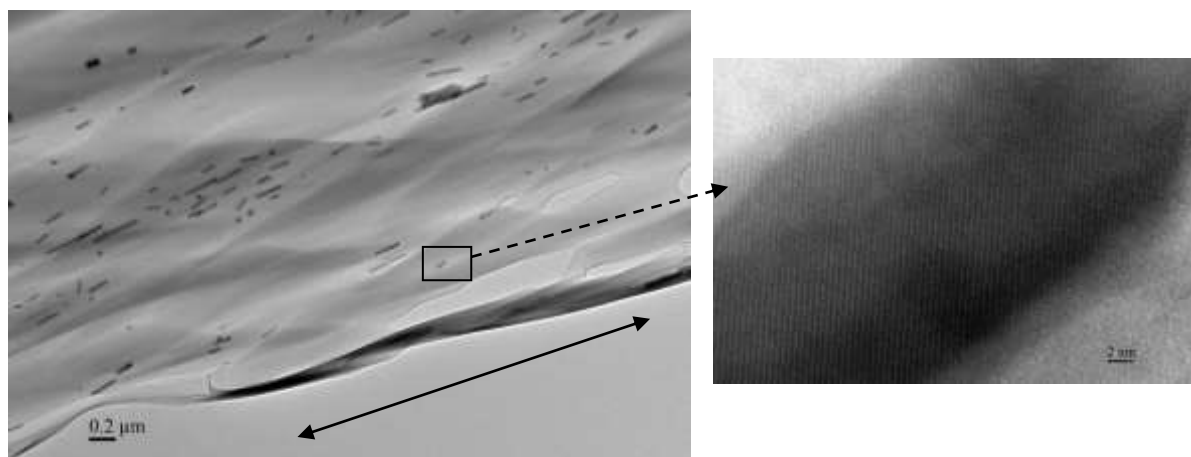


**Fig. 8.** TEM and HRTEM micrographs of nano-crystals within the SiP1.5 millimeter-sized rod. The rod-drawing direction is symbolized by a double arrow.

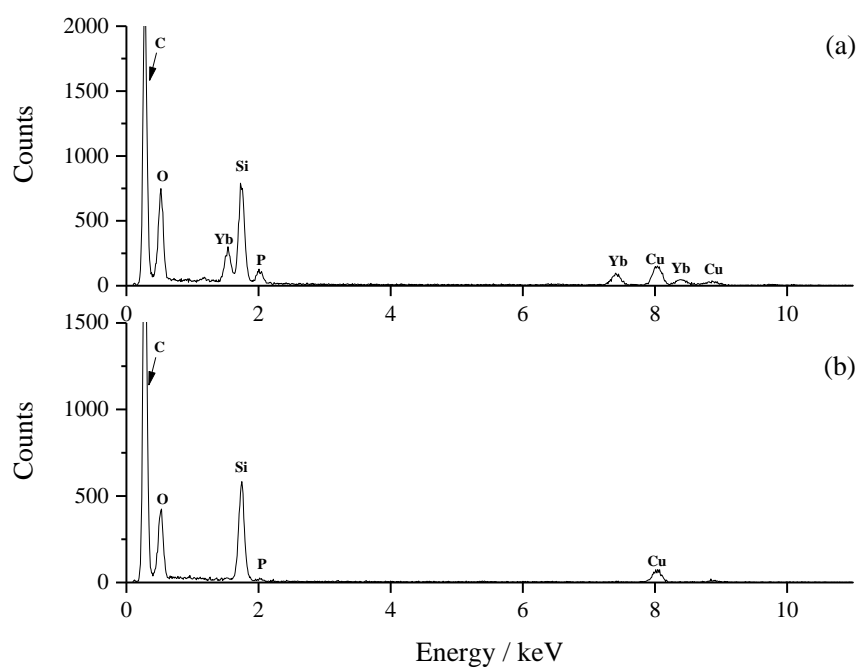


**Fig. 9.** Corresponding EDX spectra taken in scanning mode (STEM) of the nano-cylinder (a) and far from this particle (b).

Table 1 Wavenumber assignments of the Raman actives modes of  $\text{YbPO}_4$ .

$\bar{\nu} / \text{cm}^{-1}$	Assignment	Character
298	$E_g$	Rotational
328	$B_{2g}$	Internal
486	$A_{1g}$	Internal
578	$E_g$	Internal
659	$B_{1g}$	Internal
1003	$A_{1g}$	Internal
1022	$E_g$	Internal
1061	$B_{1g}$	Internal